Track-Before-Detect for Airborne Maritime Radar: Application to Real Data

Branko Ristic
School of Engineering
RMIT University
Melbourne, VIC, Australia
branko.ristic@rmit.edu.au

Du Yong Kim
School of Engineering
RMIT University
Melbourne, VIC, Australia
duyong.kim@rmit.edu.au

Luke Rosenberg
Defence Science and Technology Group
Adelaide, SA, Australia
luke.rosenberg@ieee.org

***Abstract*—Consider the problem of maritime surveillance using a high-resolution airborne radar for the detection and tracking of small surface targets. This is a challenging problem as the sea clutter is spiky with a non-Gaussian amplitude distribution and contains both temporally and spatially varying characteristics. As a possible solution, we have recently proposed a Bayesian track-before-detect algorithm, which assumes a compound K-distributed clutter model with Swerling 1 target fluctuations. This paper considers a suitable modification of this algorithm to work in the range-Doppler domain and evaluates its performance on real datasets collected by the Defence Science and Technology Group's (DSTG) Ingara X-band radar.**

I. Introduction

Radar detection and tracking of small maritime targets is difficult due to complex dynamics of the sea surface and its non-Gaussian amplitude statistics. Different environmental conditions (e.g. waves, sea swell, wind speed) and radar characteristics (e.g. range resolution, grazing angle) create different sea clutter characteristics. For higher resolutions and high sea states, the clutter amplitude distribution is characterised by longer tails and described as being spiky. Using traditional detection, these sea-spikes often cause false detections in a radar processor. Radar performance is further impacted by the spatial correlation of clutter and fluctuations in target amplitude returns.

Recently we have developed a sequential Bayesian track-before-detect (TBD) algorithm for automatic detection and tracking of small maritime targets [1]. It inputs the consecutive range-azimuth amplitude maps, and uses the compound K-distribution as a model for the clutter amplitude, while target amplitude fluctuations follow the Swerling type 1 model. Other features of this TBD algorithm include the spatial decorrelation of clutter and an online parameter estimation scheme for parameters of the K-distribution. The filter was implemented numerically using the sequential Monte Carlo method. Originally formulated for a single target, it was subsequently extended to multi-target TBD in [2]. Other extensions of this basic TBD filter include two methods for exploitation of Doppler information [3], a smoothing TBD extension [4], and utilisation of TBD after adaptive space-time processing of multichannel radar data [5].

All Bayesian methods for estimation rely on mathematical models. In this case, we have adopted two key models for the clutter amplitude distribution and the target amplitude fluctuations. The Bayesian TBD algorithms have been tested and evaluated using a high-fidelity simulator of maritime radar data [6]. The objective of this paper is to evaluate the performance of the TBD methods in the range-Doppler domain using real radar datasets collected by DSTGs Ingara X-band radar. The paper thus serves as a verification of adopted mathematical models and developed Bayesian TBD in a realistic environment.

The paper is organised as follows. Section 2 provides a preliminary overview of radar datasets. Section 3 reviews the adopted mathematical models of the radar amplitude for the cases of target absence and target presence. Section 4 presents the (single-target) Bernoulli TBD filter and its particle-filter based implementation. This section also introduces two extensions of the basic algorithm, a multi-target Bernoulli TBD and a Kullback-Leibler divergence (KLD) sampling TBD filter. Section 5 presents the numerical results obtained by processing two datasets. The conclusions and further work are summarised in Section 6.

II. Radar datasets: a preliminary overview

The collected data was collected near Kangaroo Island in South Australia, using a side-looking stripmap mode. This is illustrated in Fig. 1(a), where the arrow represents the (moving) airborne platform. The trapezoids represent the regions of the sea surface that are (sequentially) illuminated by the radar (as the observing platform moves). A target 'enters' the scene as the radar beam moves over it. The data is given as a sequence of pre-processed range-Doppler maps, where pre-processing includes motion compensation and channel balancing. We set the coherent processing interval (CPI) to 256 pulses, while the number of range cells is fixed to 19,000. Fig. 1(b) shows a typical range-Doppler amplitude map (in the log scale) in the absence of a target (only 8,000 range cells are shown). Observe that at low Doppler frequencies, the level of the sea clutter returns are stronger and more pronounced for nearer range cells.

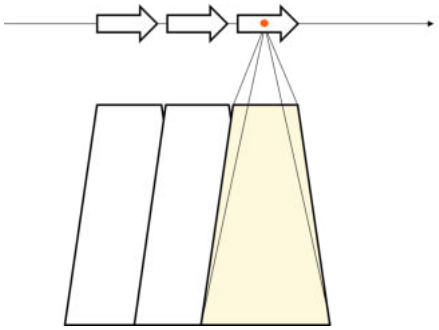

(a)

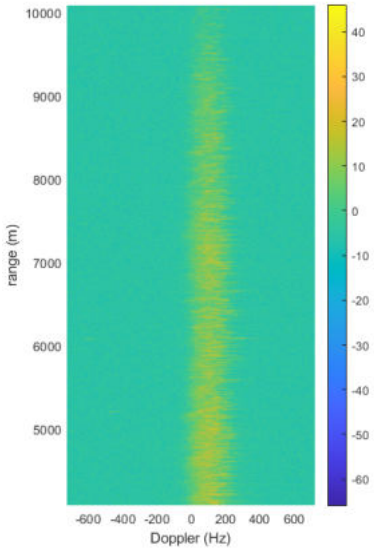

(b)

Fig. 1. (a) Stripmap data collection. (b) A typical range-Doppler amplitude map resulting from the data collection.

III. Mathematical models and a problem specification

A. Target dynamic models

A discrete-time motion model is adopted with a constant sampling period T determined as the product of the CPI and the number of pulses. The state of the target at time index k is fully characterised with the state vector $\mathbf{x}_k = [\rho_k \ \dot{\rho}_k \ \chi_k]^\intercal$, where ρ_k, $\dot{\rho}_k$ and χ_k are target range, range-rate and intensity (the energy or mean power of the target signal, which could be spread across more than one range-Doppler cell) respectively. The target state evolution satisfies the nearly constant velocity motion model [7] with the transition density given by:

$$\varphi_{k|k-1}(\mathbf{x}_k|\mathbf{x}_{k-1}) = \mathcal{N}(\mathbf{x}_k; \mathbf{F}\mathbf{x}_{k-1}, \mathbf{Q}) \tag{1}$$

where $\mathcal{N}(\mathbf{x}; \boldsymbol{\mu}, \boldsymbol{\Sigma})$ denotes the Gaussian probability density function (PDF) evaluated at $\mathbf{x}$, with mean $\boldsymbol{\mu}$ and covariance matrix $\boldsymbol{\Sigma}$. Matrices $\mathbf{F}$ and $\mathbf{Q}$ represent the transition matrix and the process noise covariance matrix respectively. They are given by:

$$\mathbf{F} = \begin{bmatrix} 1 & T & 0 \\ 0 & 1 & 0 \\ 0 & 0 & 1 \end{bmatrix}, \ \mathbf{Q} = \text{block-diag}\left(q_1 \begin{bmatrix} T^3/3 & T^2/2 \\ T^2/2 & T \end{bmatrix}, q_2 \right), \tag{2}$$

where q_1 and q_2 denote the process noise intensity in the range and amplitude domains respectively.

The presence of a target in TBD is represented by a binary random variable $\epsilon_k \in \{0, 1\}$, where by convention $\epsilon_k = 1$ means that the target is present and inversely, $\epsilon_k = 0$ means the target is absent. The dynamics of ϵ_k are modelled by a first-order two-state Markov chain, whose transitional probability matrix is given by:

$$\boldsymbol{\Pi} = \begin{bmatrix} 1 - p_\text{b} & p_\text{b} \\ 1 - p_\text{s} & p_\text{s} \end{bmatrix} \tag{3}$$

where $p_\text{b} = P\{\epsilon_{k+1} = 1 | \epsilon_k = 0\}$ and $p_\text{s} = P\{\epsilon_{k+1} = 1 | \epsilon_k = 1\}$ are referred to as the probability of *target birth* and *target survival* respectively. If the target appears at $k-1$, its state vector can be seen as a random sample from the birth density $b_{k-1}(\mathbf{x})$.

B. Measurement model

The measurement at each time k is a range-Doppler map $\mathbf{z}_k$, such as the one shown in Fig. 1(b). The measured value in cell (m, n) of the map $\mathbf{z}_k$ represents the magnitude of the complex backscatter signal where $m = 1, \ldots, \alpha$ and $n = 1, \ldots, \beta$, with α and β being the number of Doppler and range cells (in Fig. 1(b), $\alpha = 256$, $\beta = 8000$). The radar measurement model is now presented for two cases: (1) interference-only and (2) target-plus-interference.

1) Interference-only model: If no target is present in a cell of the measurement map, the measured amplitude z in the cell is due to background clutter-plus-thermal noise. This interference is formulated using the compound Gaussian model [8], which comprises a speckle component for modelling the small ripples on top of larger waves. These larger waves are then modelled by a slowly varying texture which can be assumed constant over a typical radar dwell period. The PDF of the clutter component is modelled with the K-distribution [8],

$$K(z) = \int_0^\infty R(z; \eta) G(\eta) d\eta. \tag{4}$$

where the speckle amplitude is Rayleigh distributed,

$$R(z; \eta) = \frac{2z}{\eta} \exp\left[-\frac{z^2}{\eta} \right] \tag{5}$$

with mean $\mathbb{E}[z] = \sqrt{\pi\eta}/2$. The mean square, $\mathbb{E}[z^2] = \eta$, is treated as a gamma distributed random variable,

$$G(\eta) = \frac{\eta^{\nu_0 - 1}}{b^{\nu_0} \Gamma(\nu_0)} \exp\left[-\frac{\eta}{b} \right] \tag{6}$$

where $\Gamma(\cdot)$ denotes the gamma function, $\nu_0 > 0$ is the shape parameter and $b = \mathbb{E}[\eta]/\nu_0$ is the scale. The final expression

for the K-distribution, obtained from (4), (5) and (6) is then [9]

$$K(z;\nu_0,b)=\frac{4z_0^{\nu}}{\sqrt{b}^{\nu_0+1}\,\Gamma(\nu_0)}\,\kappa_{\nu_0-1}\left(\frac{2z}{\sqrt{b}}\right) \tag{7}$$

where $\kappa_n(\cdot)$ refers to the modified Bessel function of the second kind. For $\nu_0\to\infty$, the distribution approaches the Rayleigh distribution. The PDF of clutter plus thermal noise amplitude can be also represented by a K-distribution, where the shape parameter ν_0 is replaced by an *effective* shape ν. By matching the moments of the PDF with and without thermal noise [8], one can obtain the following relationship $\nu=\nu_0\left(1+1/C\right)^2$, where C is the clutter to noise ratio (CNR). For the remainder of the paper, we will use ν as the shape parameter without explicitly defining the CNR. The term *interference* refers to the combined effect of clutter and thermal noise.

In summary, if no target is present in cell (m,n) of the measured range-Doppler map at time index k, the PDF of its amplitude is modelled by:

$$p_0^{(m,n)}(\cdot)=K(\cdot;\nu_{m,n},b_{m,n}). \tag{8}$$

In (8) we explicitly state that the shape and scale parameters of the K-distribution depend on the cell of the range-Doppler map.

2) Target-plus-interference model: When a target is present, its signature may spread to more than one range or Doppler cell. The contributing power in the (m,n)th cell at time k is related to the mean target power χ_k via the point spread function (PSF). We adopt for this purpose a Gaussian PSF,

$$d^{(m,n)}(\mathbf{x}_k)=\frac{\chi_k}{2\pi\sigma_x\sigma_y}\exp\left[-\frac{(m-D_k)^2}{2\sigma_x^2}-\frac{(n-\rho_k)^2}{2\sigma_y^2}\right] \tag{9}$$

where $D_k=2\dot{\rho}_k f_c/c$ is the Doppler frequency (f_c is the carrier frequency, c is the speed of light), and σ_x and σ_y determine the spread in Doppler and range, respectively. We model the target amplitude fluctuations as a Swerling type 1 model. Suppose a target at state $\mathbf{x}$ is present and contributing power $d>0$ to a cell of the measured map. Then the speckle amplitude in the cell of the map is Rayleigh distributed as in (5), but with the parameter $\eta+d$,

$$R(z;\eta+d)=\frac{2z}{\eta+d}\exp\left[-\frac{z^2}{\eta+d}\right], \tag{10}$$

where η is gamma distributed as in (6). The PDF of amplitude z in this case does not have an analytic expression and is given by [10]:

$$\begin{aligned}L(z;d,\nu,b)&=\int_0^{\infty}R(z;\eta+d)\,G(\eta;\nu,b)\;d\eta\\&=\frac{2z}{b^{\nu}\Gamma(\nu)}\int_0^{\infty}\frac{\eta^{\nu-1}}{\eta+d}\,\exp\left[-\frac{z^2}{\eta+d}-\frac{\eta}{b}\right]d\eta.\end{aligned} \tag{11}$$

The amplitude PDF of a Swerling 1 target in K-distributed clutter plus noise will be referred to as the L-distribution. Because this integral has no analytic solution, it will be computed numerically. If $\nu\to\infty$, the gamma distribution (6) approaches a delta function and the L-distribution becomes Rayleigh as in (10).

In summary, if a target in state $\mathbf{x}_k$ is contributing power $d_k^{(m,n)}(\mathbf{x}_k)$ to the cell (m,n) at time index k, the PDF of the measured amplitude in this cell is given by:

$$p_1^{(m,n)}(\cdot|\mathbf{x}_k)=L\left(\cdot;d_k^{(m,n)}(\mathbf{x}_k),\nu_{m,n},b_{m,n}\right). \tag{12}$$

IV. Track-Before-Detect Algorithm

The fundamental building block of TBD algorithm is the Bernoulli TBD filter [1], [11], as the optimal (in the Bayesian sense) recursive estimator for an appearing / disappearing target.

A. The Bernoulli TBD filter

The Bernoulli TBD filter propagates two quantities over time. The first is the posterior probability of target presence $q_{k|k}=P\{\epsilon_k=1|\mathbf{z}_{1:k}\}$, where $\mathbf{z}_k$ denotes the measured amplitude map at time index n consisting of $\alpha\times\beta$ cells, discussed in Section III-B, and $\mathbf{z}_{1:k}\equiv\mathbf{z}_1,\ldots,\mathbf{z}_k$ is the sequence of measured maps from the initial index 1 to the current time index k. The second quantity is the posterior spatial probability distribution $s_{k|k}(\mathbf{x})=p(\mathbf{x}_k|\mathbf{z}_{1:k})$, conditioned on target existence. If at time $k-1$, both $q_{k-1|k-1}$ and $s_{k-1|k-1}(\mathbf{x})$ are available, then the recursive computation of $q_{k|k}$ and $s_{k|k}(\mathbf{x})$ can be carried out in two steps, prediction and update.

The prediction equations of the Bernoulli filter are as follows [11]:

$$q_{k|k-1}=p_b\left(1-q_{k-1|k-1}\right)+p_s\,q_{k-1|k-1} \tag{13}$$

$$s_{k|k-1}(\mathbf{x})=\frac{p_b\left(1-q_{k-1|k-1}\right)\int\varphi_{k|k-1}(\mathbf{x}|\mathbf{x}')\,b_{k-1}(\mathbf{x}')d\mathbf{x}'}{q_{k|k-1}}+\frac{p_s\,q_{k-1|k-1}\int\varphi_{k|k-1}(\mathbf{x}|\mathbf{x}')\,s_{k-1|k-1}(\mathbf{x}')d\mathbf{x}'}{q_{k|k-1}}, \tag{14}$$

where

- p_{s} and p_{b} are the probability of target survival and the probability of target birth, respectively;
- $b_{k-1}(\mathbf{x})$, referred to as the target birth density, is the probability density over the state space which models the state of the target if it has appeared at time index $k-1$. A practical design of $b_{k-1}(\mathbf{x})$ will be discussed in Section IV-A2.

The update equations are given by:

$$q_{k|k}=\frac{q_{k|k-1}\int\ell_k(\mathbf{z}_k|\mathbf{x})\,s_{k|k-1}(\mathbf{x})\,d\mathbf{x}}{1-q_{k|k-1}+q_{k|k-1}\int\ell_k(\mathbf{z}_k|\mathbf{x})\,s_{k|k-1}(\mathbf{x})\,d\mathbf{x}} \tag{15}$$

$$s_{k|k}(\mathbf{x})=\frac{\ell_k(\mathbf{z}_k|\mathbf{x})\,s_{k|k-1}(\mathbf{x})}{\int\ell_k(\mathbf{z}_k|\mathbf{x})\,s_{k|k-1}(\mathbf{x})\,d\mathbf{x}} \tag{16}$$

where $\ell_k(\mathbf{z}_k|\mathbf{x}_k)$ is the likelihood ratio defined as:

$$\ell_k(\mathbf{z}_k|\mathbf{x}_k)=\prod_{m=1}^{\alpha}\prod_{n=1}^{\beta}\frac{p_1^{(m,n)}\left(z_{m,n}|\mathbf{x}_k\right)}{p_0^{(m,n)}\left(z_{m,n}\right)} \tag{17}$$

with likelihood functions $p_1^{(m,n)}(\cdot|\mathbf{x}_k)$ and $p_0^{(m,n)}(\cdot)$ introduced in (12) and (8) respectively. The likelihood ratio (17) plays a crucial role in the Bernoulli filter for TBD. In practice, the parameters $\nu_{m,n}$ and $b_{n,m}$, which are necessary for the computation of the likelihood ratio, are unknown. Their estimation will be discussed in Section IV-A3.

1) Implementation of the Bernoulli TBD filter: The probability of target presence $q_{k|k}$ is a scalar and its prediction and update steps are given by analytic expressions (13) and (15). The main problem is how to represent and propagate in time the posterior spatial density $s_{k|k}(\mathbf{x})$. For this purpose, we adopt the sequential Monte Carlo (SMC) method [12] and implement the Bernoulli TBD filter as a particle filter, following [11, Sec. VIII.A].

Let the posterior $s_{k-1|k-1}(\mathbf{x})$ be represented by $N \gg 1$ random samples or particles $\{w_{k-1}^{(j)}, \mathbf{x}_{k-1}^{(j)}\}_{j=1}^{N}$. Here $\mathbf{x}_{k-1}^{(j)}$ is the state of the jth particle, while $w_{k-1}^{(j)}$ is its weight. The weights are non-negative and sum to 1. The Monte Carlo representation of $s_{k-1|k-1}(\mathbf{x})$ can be expressed as:

$$s_{k-1|k-1}(\mathbf{x}) \approx \sum_{j=1}^{N} w_{k-1}^{(j)} \delta_{\mathbf{x}_{k-1}^{(j)}}(\mathbf{x}) \tag{18}$$

where $\delta_{\mathbf{x}_k}(\mathbf{x})$ is the Dirac delta function focused at $\mathbf{x}_k$. Similarly, let the birth density $b_{k-1}(\mathbf{x})$ be represented by weighted particles $\{w_{k-1,b}^{(j)}, \mathbf{x}_{k-1,b}^{(j)}\}_{j=1}^{N_\mathrm{b}}$. Then, according to (14), the Monte Carlo approximation of $s_{k|k-1}(\mathbf{x})$ is a union of two sets of weighted predicted particles, i.e.

$$\{w_{k|k-1}^{(j)}, \mathbf{x}_{k|k-1}^{(j)}\}_{j=1}^{N} \bigcup \{w_{k|k-1,b}^{(j)}, \mathbf{x}_{k|k-1,b}^{(j)}\}_{j=1}^{N_\mathrm{b}}. \tag{19}$$

Adopting the proposal density of the particle filter to be the transition density in (1), then from (14) it follows that the weights in (19) are given by:

$$w_{k|k-1}^{(j)} = \frac{p_\mathrm{s} q_{k-1|k-1}}{q_{k|k-1}} w_{k-1}^{(j)} \tag{20}$$

$$w_{k|k-1,b}^{(j)} = \frac{p_\mathrm{b}(1 - q_{k-1|k-1})}{q_{k|k-1}} w_{k-1,b}^{(j)}. \tag{21}$$

The set of particles in (19) can be written as $\{w_{k|k-1}^{(j)}, \mathbf{x}_{k|k-1}^{(j)}\}_{j=1}^{N_{k|k-1}}$, where $N_{k|k-1} = N + N_\mathrm{b}$.

In the update step, observe that the integral can be approximated by a sum, i.e.

$$\int \ell_k(\mathbf{z}_k|\mathbf{x})\, s_{k|k-1}(\mathbf{x}) d\mathbf{x} \approx \sum_{j=1}^{N_{k|k-1}} \ell_k\left(\mathbf{z}_k|\mathbf{x}_{k|k-1}^{(j)}\right) w_{k|k-1}^{(j)},$$

abbreviated as $I(\mathbf{z}_k)$. If we represent $s_{k|k}(\mathbf{x})$ by a set of weighted particles $\{w_{k|k}^{(j)}, \mathbf{x}_{k|k}^{(j)}\}_{j=1}^{N_{k|k-1}}$, then $w_{k|k}^{(j)} = \ell_k\left(\mathbf{z}_k|\mathbf{x}_{k|k-1}^{(j)}\right)/I(\mathbf{z}_k)$ and $\mathbf{x}_{k|k}^{(j)} = \mathbf{x}_{k|k-1}^{(j)}$, for $j = 1, \ldots, N_{k|k-1}$. The last step in the implementation is the resampling step, where we select N samples from $\{w_{k|k}^{(j)}, \mathbf{x}_{k|k}^{(j)}\}_{j=1}^{N_{k|k-1}}$. Resampling serves two purposes: (i) it keeps the number of particles constant in time; (ii) it eliminates (in the probabilistic sense) the particles with small weights, and multiplies the particles with large weights [12].

Next we describe how the particles from the birth density are created and how the shape and scale parameters of the K-distribution are estimated. These two features of the Bernoulli TBD particle filter differ from [3]. The main reason for this change is that in the real data, shown by Fig. 1(b), the intensity of the Doppler spectrum reduces with range.

2) The formation of birth density particles: One of the most important aspects of Bernoulli TBD is how to form the particles that represent the birth density $b_{k-1}(\mathbf{x})$. The current implementation of this step requires first to estimate the mean background of the interference in the range-Doppler map $\mathbf{z}_{k-1}$. This step is carried out using a 2D cell-averaging process with the interference level in the cell under test (CUT) (m, n) estimated as the average value of the amplitudes in a block of cells determined by a hollow two-dimensional window of size $W_\mathrm{D} \times W_\rho$, centered at the CUT. These cells are referred to as the training cells, with the window for averaging shown graphically in Fig. 2(a). The cells immediately adjacent to the CUT are referred to as *guard cells* and are not included because of potential target signal leakage. The estimated mean interference background corresponding to the range-Doppler map in Fig. 1(b) is shown in Fig. 2(b). The guard cells window is ± 2 in both the range and Doppler directions. The training cell window in range direction is ± 500, while in Doppler is set to ± 10 cells.

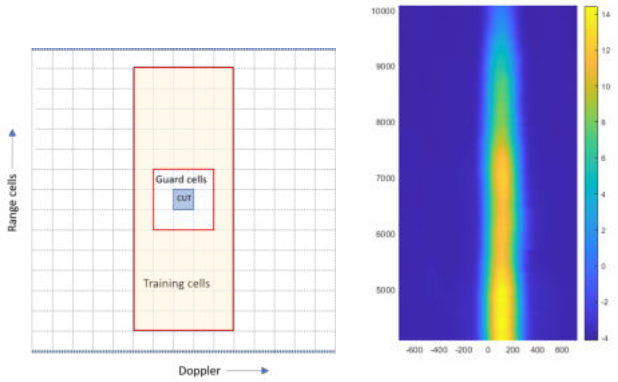

(a) (b)

Fig. 2. Cell-averaging: (a) the averaging window (indicated in ochre colour) for the CUT (indicated in blue). (b) Estimated mean interference floor corresponding to the range-Doppler map in Fig. 1(b).

The next step in the formation of the birth density particles is to determine the cells of the range-Doppler map that are characterised by an amplitude greater than the estimated mean background, multiplied by a coefficient $\hbar > 0$. In those cells we place the birth density particles whose range and range-rate components correspond to the range and Doppler values of each cell. The intensity component of each birth particle is a random draw from a positive distribution, adopted as the log-normal for convenience.

3) Estimation of the shape and scale parameters: In order to compute the likelihood ratio $\ell_k\left(\mathbf{z}_k|\mathbf{x}_{k|k-1}^{(j)}\right)$, it is necessary to find the cell of the range-Doppler map in which the jth

particle $\mathbf{x}_{k|k-1}^{(j)} = [\rho_{k|k-1}^{(j)},\ \dot{\rho}_{k|k-1}^{(j)},\ \chi_{k|k-1}^{(j)}]$ lies. Suppose it is in the (m,n)th cell, then the estimates $\nu_{m,n}$ and $b_{m,n}$ can be computed using the moment based method [13]. This requires the collection of a set of amplitude values from the range-Doppler map $\mathbf{z}_k$, inside a two-dimensional window centered at the (m,n)th cell. The window contains a hole (i.e. guard cells) centered at the (m,n)th cell, similar to the cell averaging window in Fig. 2(a). This was done because the guard cells could contain the contribution from the target. Let $z_1, \cdots, z_L$ be such a set of amplitude values. The first and the second sample moments are estimated as:

$$\widehat{m}_1 = \frac{1}{L}\sum_{l=1}^{L} z_l, \qquad \widehat{m}_2 = \frac{1}{L}\sum_{l=1}^{L} z_l^2. \tag{22}$$

Assuming that samples $z_1, \cdots, z_L$ are random draws from the K-distribution, then an approximate closed form solution for the shape parameter is [13]:

$$\widehat{\nu}_{m,n} = \frac{1}{4}\left[\ln\left(\frac{\pi\,\widehat{m}_2}{4\,\widehat{m}_1^2}\right)\right]^{-1}, \tag{23}$$

while the scale estimate is computed as $\widehat{b}_{m,n} = \widehat{m}_2 \diagup \widehat{\nu}_{m,n}$.

B. Multi-target Bernoulli TBD tracker

It is imperative to develop a multi-target TBD tracking algorithm when dealing with real datasets, even if there is a single target present because occasional false tracks are inevitable. We have developed a Bernoulli multi-target TBD (BMT-TBD) algorithm following [2] and assuming that all existing tracks are well separated in range.

Suppose at time $k-1$ there are C_{k-1} tracks. Track with index τ, such that $\tau = 1, \ldots, C_{k-1}$, is specified by $\mathcal{T}_{k-1}^{(\tau)} = \left(\mathcal{L}^{(\tau)}, q_{k-1|k-1}^{(\tau)}, s_{k-1|k-1}^{(\tau)}\right)$, where $\mathcal{L}^{(\tau)}$ is a unique track label, $q_{k-1|k-1}^{(\tau)}$ is the posterior probability of the τth target being present and $s_{k-1|k-1}^{(\tau)}(\cdot)$ is the posterior PDF of the τth track over the state space $\mathcal{X}$. The set of all tracks at $k-1$ is then specified as

$$\mathcal{T}_{k-1} = \left\{\left(\mathcal{L}^{(\tau)}, q_{k-1|k-1}^{(\tau)}, s_{k-1|k-1}^{(\tau)}\right)\right\}_{1\le\tau\le C_{k-1}}. \tag{24}$$

At the next time step k, when a new measured range-Doppler map $\mathbf{z}_k$ becomes available, the BMT-TBD is run using the processing steps listed in Alg. 1.

Algorithm 1 Processing steps of the BMT-TBD at time k

1: **Input:** $\mathcal{T}_{k-1}$, $\mathbf{z}_k$
2: $\mathcal{T}_{k|k-1}$ = Predict_Tracks ($\mathcal{T}_{k-1}$)
3: $[\mathcal{T}_{k|k}, \mathbf{z}_k^*]$ = Update_Tracks ($\mathcal{T}_{k|k-1}$, $\mathbf{z}_k$)
4: $\widetilde{\mathcal{T}}_k$ = Track_Management ($\mathcal{T}_{k|k}$)
5: Track_Reporting ($\widetilde{\mathcal{T}}_k$)
6: $\mathcal{V}_k$ = Init_NewTracks ($\mathbf{z}_k^*$)
7: $\mathcal{T}_k$ = Track_Union ($\widetilde{\mathcal{T}}_k$, $\mathcal{V}_k$)
8: **Output:** $\mathcal{T}_k$

Initially, at $k=1$, $\mathcal{T}_{k-1} = \emptyset$. In line 2 of Alg. 1, each track $\tau = 1, \ldots, |\mathcal{T}_{k-1}|$ is predicted as follows [14, p.662]:

$$q_{k|k-1}^{(\tau)} = p_s \cdot q_{k-1|k-1}^{(\tau)}, \tag{25}$$

$$s_{k|k-1}^{(\tau)}(\mathbf{x}) = \int \varphi_{k|k-1}(\mathbf{x}|\mathbf{x}')\, s_{k-1|k-1}^{(\tau)}(\mathbf{x}')\, d\mathbf{x}', \tag{26}$$

while the track label does not change.

If track τ is well separated from all other tracks in $\mathcal{T}_{k|k-1}$, the computation of the likelihood function for this track can be approximated with

$$\ell_\tau(\mathbf{z}_k|\mathbf{x}) \approx \prod_{m\in\mathcal{S}_\tau(D)}\prod_{n\in\mathcal{S}_\tau(\rho)} \frac{L\left(z^{(m,n)}; d^{(m,n)}(\mathbf{x}), \nu_{m,n}, b_{m,n}\right)}{K\left(z^{(m,n)}; \nu_{m,n}, b_{m,n}\right)} \tag{27}$$

where $\mathcal{S}_\tau(D)$ and $\mathcal{S}_\tau(\rho)$ are the sets of cell indices, covering the support of the PDF $s_{k|k-1}^{(\tau)}(\mathbf{x})$, in the Doppler and range directions, respectively. The support is determined by the spread parameters σ_x and σ_y introduced in (9).

Then the update equations for the τth track are as follows [15]:

$$q_{k|k}^{(\tau)} = \frac{q_{k|k-1}^{(\tau)} \int \ell_\tau(\mathbf{z}_k|\mathbf{x})\, s_{k|k-1}^{(\tau)}(\mathbf{x})\, d\mathbf{x}}{1 - q_{k|k-1}^{(\tau)} + q_{k|k-1}^{(\tau)} \int \ell_\tau(\mathbf{z}_k|\mathbf{x})\, s_{k|k-1}^{(\tau)}(\mathbf{x})\, d\mathbf{x}} \tag{28}$$

$$s_{k|k}^{(\tau)}(\mathbf{x}) = \frac{\ell_\tau(\mathbf{z}_k|\mathbf{x})\, s_{k|k-1}^{(\tau)}(\mathbf{x})}{\int \ell_\tau(\mathbf{z}_k|\mathbf{x})\, s_{k|k-1}^{(\tau)}(\mathbf{x})\, d\mathbf{x}}. \tag{29}$$

During the update of tracks, the range-Doppler map is modified and denoted $\mathbf{z}_k^*$. This modification involves setting those cells of the original range-Doppler map $\mathbf{z}_k$, that have been used in the computation of the likelihoods $\ell_\tau(\mathbf{z}_k|\mathbf{x})$, for $\tau = 1, \ldots, |\mathcal{T}_{k|k-1}|$ to zero in $\mathbf{z}_k^*$. Note that $\mathbf{z}_k^*$ is used in line 6 of Alg. 1 to initiate new tracks, whose status is *tentative*.

Track management in line 4 of Alg. 1 involves promoting good *tentative* tracks (with a high value of $q_{k|k}^{(\tau)}$) to the *confirmed* status and demoting *confirmed* tracks or deleting *tentative* tracks with a low value of $q_{k|k}^{(\tau)}$. Also, track management performs merging of the tracks that are close to each other in range. This merging step was introduced because the BMT-TBD tracker would form multiple tracks on a large target due to the high range-resolution. This effect is illustrated in Fig. 3. Part (a) of this figure shows a typical signature of a large target. The target extends in range more than 25 meters, and appears to have a few dominant scattering points. This is clearly different from the Gaussian point spread function that was assumed in (9). The consequence of this discrepancy is that multiple tracks are typically formed on the extended target, as illustrated in Fig. 3(b). Track management will merge all tracks which are close to each other.

Track reporting (in line 5 of Alg. 1) is based on track status, where only confirmed tracks are reported. New tracks are initialised in line 6 of Alg. 1 with all initial tracks given a *tentative* status.

Track initialisation is similar to the procedure described in Sec. IV-A2 and [2]. The range-Doppler map $\mathbf{z}_k^*$ is compared to a threshold, computed as a multiple of the interference

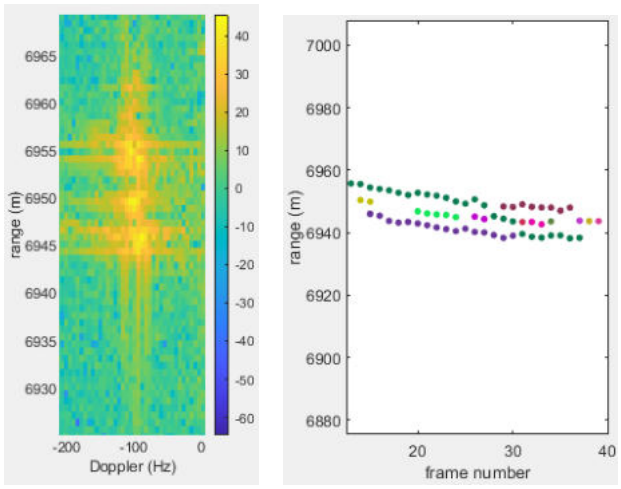

(a) (b)

Fig. 3. Target signature with a high-resolution radar: (a) target spreads (extends) over many range cells; (b) multiple-tracks on the extended target.

background (the mean background computation explained in Sec. IV-A2). Subsequently, all cells of the map, which are above this threshold, are grouped into connected components. Each connected component forms a new track, whose spatial density $s_{k|k}^{(\tau)}(\mathbf{x})$ is approximated by "birth" particles. The range and Doppler components of these particles correspond to the range and Doppler values of the cells in the particular connected component. Intensity values of the particles are a random draw from a log-normal distribution. For every track $\mathcal{T}_k^{(\tau)}$, the posterior $s_{k|k}^{(\tau)}(\mathbf{x})$ is approximated by particles, as discussed in Sec. IV-A1.

C. Kullback–Leibler distance sampling

Kullback–Leibler distance (KLD) sampling was introduced in order to adapt the sample size in a particle approximation of each track posterior spatial distribution [16]. Thus, the spatial density $s_{k|k}^{(\tau)}(\mathbf{x})$ of every track is approximated with a different number of particles. The key idea of the KLD-sampling method is to bound the approximation error introduced by the sample-based representation of the particle filter. The name KLD-sampling is due to the fact that the approximation error is measured using the KLD. The adaptation approach chooses a small number of samples if the spatial density is focused on a small part of the state space, and conversely, chooses a large number of samples if the state uncertainty is high [17].

The state space needs to be divided (discretised) into equal sized bins. The KLD sampling particle filter constantly monitors the number of bins that are occupied with particles. This number determines the number of particles in combination with the input parameters that define the desired accuracy. Psuedo-code of the KLD sampling particle filter for the τth track is given in Alg. 2. The parameters of this algorithm are the accuracy parameters ε and δ, the bin size Δ, and the minimum number of particles $n_{\min}$. The input to the algorithm are the particle approximation $S_{k-1}^{(\tau)}$ of $s_{k|k}^{(\tau)}(\mathbf{x})$ and the measured range-Doppler map $\mathbf{z}_k$. Line 2 performs initialisation, followed by a while-loop which terminates when the number of particles is sufficient. Line 11, which calculates the number of particles, features κ, ε and $z_{1-\delta}$. Variable κ in Alg. 2 is the counter of occupied bins. Parameters ε and $z_{1-\delta}$ determine the accuracy of the sample approximation in the following sense: $1-\delta$ is the probability that the KLD between the sample approximation and the true posterior distribution is less than ε [16].

Algorithm 2 KLD sampling algorithm for track τ at time k

1: **Input:** $S_{k-1}^{(\tau)} = \{(w_{k-1}^{(\tau,j)}, \mathbf{x}_{k-1}^{(\tau,j)}\}_{j=1}^{N_{k-1}^{\tau}}$, $\mathbf{z}_k$
2: Initialise: $S_k^{(\tau)} = \emptyset$, $n = 0$, $n_x = 1$, $\kappa = 0$
3: **while** $n < n_x$ & $n < n_{\min}$ **do**
4: Sample particle index j^* from discrete distrib. $S_{k-1}^{(\tau)}$
5: Sample $\mathbf{x}_k^{(\tau,j^*)}$ from $\varphi_{k|k-1}\left(\cdot\,|\mathbf{x}_{k-1}^{(\tau,j^*)}\right)$
6: Compute weight $w_k^{(\tau,j^*)} = \ell_k\left(\mathbf{z}_k|\mathbf{x}_k^{(\tau,j^*)}\right) p_s\, w_{k-1}^{(\tau,j^*)}$
7: $S_k^{(\tau)} = S_k^{(\tau)} \cup \{(w_k^{(\tau,j^*)}, \mathbf{x}_k^{(\tau,j^*)})\}$
8: **if** $\mathbf{x}_k^{(\tau,j^*)}$ falls into empty bin b **then**
9: Increase the counter of occupied bins: $\kappa \leftarrow \kappa + 1$
10: Mark bin b as being occupied
11: Calculate [16]

$$n_x = \frac{\kappa - 1}{2\varepsilon}\left[1 - \frac{2}{9(\kappa-1)} + \sqrt{\frac{2}{9(\kappa-1)}}z_{1-\delta}\right]^3$$

12: **end if**
13: $n \leftarrow n + 1$
14: **end while**
15: $N_k^{\tau} \leftarrow n$
16: Normalise: $w_k^{(\tau,j)} \leftarrow w_k^{(\tau,j)} / \sum_{\ell=1}^{N_k^{\tau}} w_k^{(\tau,\ell)}$, $j = 1\ldots, N_k^{\tau}$
17: **Output:** $S_k^{(\tau)} = \{(w_k^{(\tau,j)}, \mathbf{x}_k^{(\tau,j)}\}_{j=1}^{N_k^{\tau}}$

A detailed study and performance analysis of KLD sampling TBD using simulated data is presented in [17].

V. Numerical results

Parameters of the target birth model. The parameters which feature in (3) are set to $p_b = 0.01$ and $p_s = 0.95$. This choice reflects the fact that targets appear rarely, and when they appear, they tend to exist for only a short time. Estimation of the interference background level using the cell-averaging window was described in Section IV-A2 with the window size the same as described in relation to Fig. 2(b). The multiplier $\hbar$ determines the cells of the range-Doppler map where the birth particle are to be formed (i.e. new tracks initialised). This multiplier is determined automatically so that at most five new tracks (i.e. five connected components after thresholding) are initialised in each radar frame. The probability of target presence for a new (initialised) track τ is set to $q_k^{(\tau)} = 0.02$. Each new track is given a *tentative* status.

The window used for estimation of $\nu_{m,n}$ and $b_{m,n}$. The window is the same as the cell averaging window used for estimation of the interference background level.

TABLE I
PARAMETERS USED IN DATA COLLECTION.

Parameter	Value
Platform speed	83.38 m/s
Radar carrier frequency	10.1 GHz
Bandwidth	200 MHz
Pulse repetition frequency	1450 Hz
Number of range bins	27121

Parameters related to track management. A tentative track τ is promoted to the confirmed status when $q_{k|k}^{(\tau)} > 0.8$. A confirmed track τ is demoted to the tentative status if $q_{k|k}^{(\tau)}$ falls below 0.6. A tentative track τ is deleted if $q^{(\tau)} < 0.02$. Finally, two tracks are merged if their separation in range is less than 30 meters.

The number of particles. We have developed two versions of the Multi-target Bernoulli TBD tracker: (1) Using a fixed number of $N = 300$ particles per track, referred to as the BMT-TBD-F tracker; (2) Using KLD sampling for automatic and adaptive determination of the number of particles, referred to as BMT-TBD-A. The parameters used for KLD sampling are: $\Delta = 10 \times 10$ cells in the range-Doppler state space, with $n_{\min} = 10$, $\varepsilon = 0.02$ and $\delta = 0.25$.

A. TBD output

Two datasets are studied in this section with the radar parameters used in data collection are given in Table I. The ground truth for both datasets is unknown.

1) Dataset 1: We have processed the range cells from 4001 to 16000 with a duration of 42 range-Doppler frames. The two BMT-TBD algorithms performed almost identically: they reported only one track during the observation period, with the target initial range of 6962 m, reducing over time to 6932 m. The BMT-TBD-F reported the track for the first time at frame number 8, while BMT-TBD-A did the same at frame number 9. Both trackers reported the track for the last time at frame number 30. The average number of particles per track in the BMT-TBD-A was 383.

Fig. 4 shows the range-Doppler amplitude map and the initialised track at frame 9 (when the track was established by BMT-TBD-A) in the range–range-rate domain. The radial velocity of the target is small, and hence the track appears at low Doppler frequency, masked by high sea clutter. The track remains in this region until $k = 30$, when it was reported for the last time. The output of the two BMT-TBD tracking algorithms in the range-time is presented in Fig. 5. As we already stated, the results from two TBD algorithms are almost identical.

2) Dataset 2: In this dataset, we have processed range cells from 5001 to 18000. The outputs of the two TBD algorithms are identical. At frame number 11, a false track is declared at range 5181 m, then at frame number 19, another false track is declared at range 4121 m. At the same frame 19, a valid target track is declared at range 8180 m. This track existed and is reported until the very last frame (number 42) of this dataset. The radial velocity of this target is fairly small and hence the target range at the last scan is about 8175 m (a radial movement of about 5 meters). One more target is captured in this dataset. It was fist detected in the frame number 22, at range 8930 m. The target is weak and hence the track only existed for 4 scans. The target is again detected and tracked (under a new label) from frame number 28 to 34. The average number of particles used per track by the BMT-TBD in this case was 415.

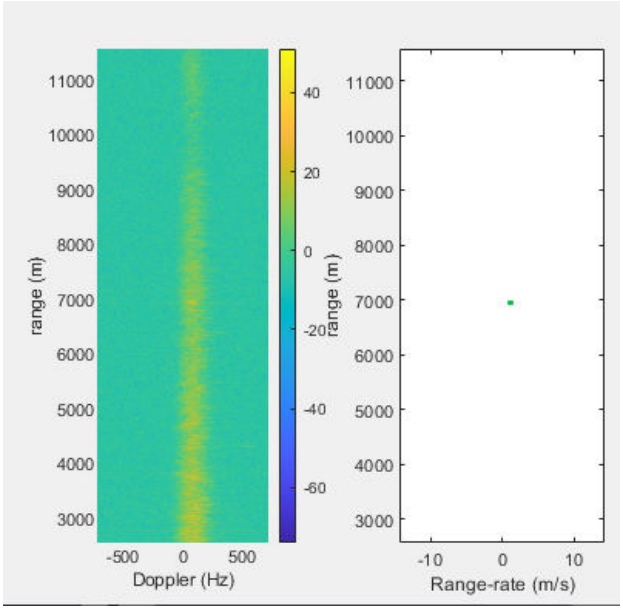

(a) (b)

Fig. 4. First dataset: (a) Range-Doppler amplitude map. (b) Established track in the range–range-rate domain.

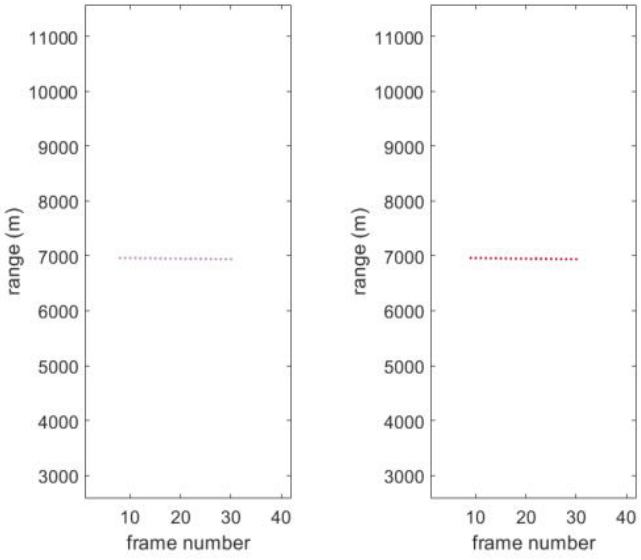

(a) (b)

Fig. 5. First dataset: Range-time plots obtained using (a) BMT-TBD-F tracker. (b) BMT-TBD-A tracker.

Fig. 6(a) shows the range-Doppler amplitude map, while part (b) shows the two tracks from frame 22 in the range–range-rate domain. This is the frame when two valid tracks are reported. The radial velocities of both targets are small, and hence they are masked by high sea clutter. The resulting range-time plots obtained as the output of the two BMT-TBD tracking algorithms are presented in Fig. 7.

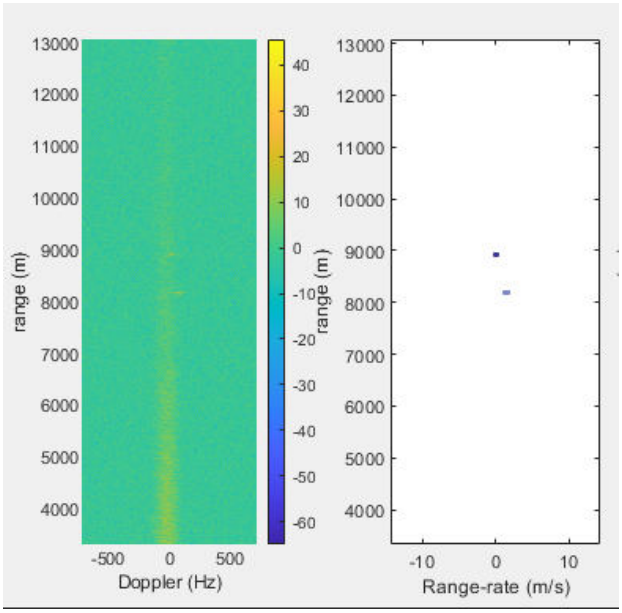

(a) (b)

Fig. 6. Second dataset: (a) Range-Doppler amplitude map. (b) Established track in the range–range-rate domain.

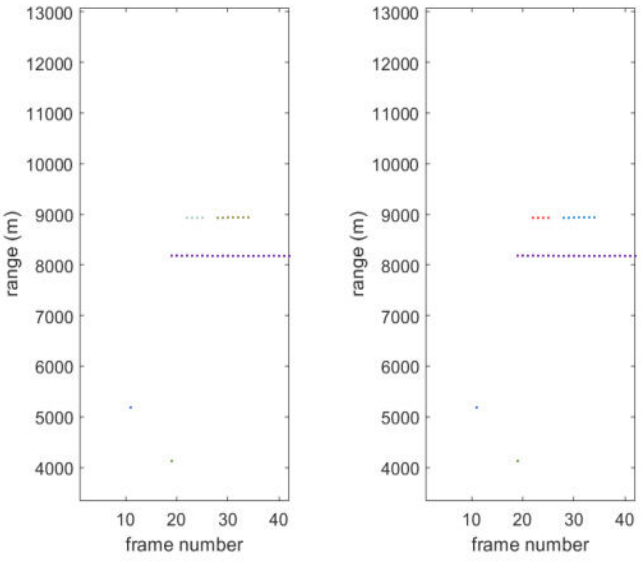

(a) (b)

Fig. 7. Second dataset: Range-time plots obtained using (a) BMT-TBD-F tracker. (b) BMT-TBD-A tracker.

VI. Conclusion

The paper presented the results obtained when two Bayesian multi-target TBD algorithms were applied to real radar datasets, collected by DSTG during maritime radar trials. The results indicate that TBD algorithms can detect and track the true targets accurately, using only a few hundred particles. Occasionally, very short (at most one frame long) false tracks are reported. Future work will consider automatic tuning of TBD parameters, faster (real-time) execution of the algorithms, and more appropriate target models (e.g. taking into consideration the target extent in range).

Acknowledgement

B. Ristic and D. Y. Kim acknowledge the funding provided by the Defence Science and Technology group under the Research Agreement with RMIT University, titled "Track-Before-Detect for Maritime Radar".

References

[1] B. Ristic, L. Rosenberg, D. Y. Kim, X. Wang, and J. Williams, "A Bernoulli track-before-detect filter for maritime radar," *IET Radar Sonar Navigation*, 2020.

[2] D. Y. Kim, B. Ristic, R. Guan, and L. Rosenberg, "A Bernoulli track-before-detect filter for interacting targets in maritime radar," *IEEE Transactions on Aerospace and Electronic Systems*, vol. 57, no. 3, pp. 1981–1991, 2021.

[3] B. Ristic, D. Y. Kim, L. Rosenberg, and R. Guan, "Exploiting Doppler in Bernoulli track-before-detect for a scanning maritime radar," *IEEE Transactions on Aerospace and Electronic Systems*, vol. 58, no. 1, pp. 720–728, 2022.

[4] B. Ristic, R. Guan, D. Y. Kim, and L. Rosenberg, "Bernoulli track-before-detect smoothing for maritime radar," *IET Radar, Sonar & Navigation*, 2022.

[5] D. Y. Kim, L. Rosenberg, B. Ristic, and R. Guan, "Track-before-detect using an airborne multi-channel radar in the maritime domain," *IEEE Transactions on Aerospace and Electronic Systems*, vol. 59, no. 3, 2023.

[6] L. Rosenberg, S. Watts, and S. Bocquet, "Scanning radar simulation in the maritime environment," in *2020 IEEE Radar Conference (RadarConf20)*, pp. 1–6, IEEE, 2020.

[7] Y. Bar-Shalom, X. R. Li, and T. Kirubarajan, *Estimation with Applications to Tracking and Navigation*. John Wiley & Sons, 2001.

[8] K. D. Ward, R. J. A. Tough, and S. Watts, *Sea Clutter: Scattering, the K-Distribution and Radar Performance*. The Institute of Engineering Technology, second ed., 2013.

[9] P. Z. Peebles, *Radar principles*. Wiley, 1998.

[10] E. Brekke, O. Hallingstad, and J. Glattetre, "Tracking small targets in heavy-tailed clutter using amplitude information," *IEEE Journal of Oceanic Engineering*, vol. 35, no. 2, pp. 314–329, 2010.

[11] B. Ristic, B.-T. Vo, B.-N. Vo, and A. Farina, "A tutorial on Bernoulli filters: theory, implementation and applications," *IEEE Trans. on Signal Processing*, vol. 61, no. 13, pp. 3406–3430, 2013.

[12] B. Ristic, S. Arulampalam, and N. Gordon, *Beyond the Kalman filter: Particle filters for tracking applications*. Artech House, 2004.

[13] D. A. Abraham and A. P. Lyons, "Novel physical interpretations of K-distributed reverberation," *IEEE Journal of Oceanic Engineering*, vol. 27, no. 4, pp. 800–813, 2002.

[14] R. Mahler, *Statistical Multisource Multitarget Information Fusion*. Artech House, 2007.

[15] B.-N. Vo, B.-T. Vo, N.-T. Pham, and D. Suter, "Joint detection and estimation of multiple objects from image observations," *IEEE Trans. Signal Processing*, vol. 58, no. 10, pp. 5129–5141, 2010.

[16] D. Fox, "Adapting the sample size in particle filters through KLD-sampling," *The international Journal of robotics research*, vol. 22, no. 12, pp. 985–1003, 2003.

[17] D. Y. Kim, L. Rosenberg, B. Ristic, and R. Guan, "Track-before-detect with Kullback-Leibler divergence sampling," in *2023 IEEE Radar Conference (RadarConf23)*, pp. 1–6, 2023.